Hopping and Rolling Locomotion with Spherical Tensegrity Robots

Kyunam Kim, Lee-Huang Chen, Brian Cera, Mallory Daly, Edward Zhu, Julien Despois,
Adrian K. Agogino, Vytas SunSpiral, and Alice M. Agogino, *Member, IEEE*

Abstract— This work presents a 10 kg tensegrity ball probe that can quickly and precisely deliver a 1 kg payload over a 1 km distance on the Moon by combining cable-driven rolling and thruster-based hopping. Previous research has shown that cable-driven rolling is effective for precise positioning, even in rough terrain. However, traveling large distances using thruster-based hopping, which is made feasible by the lightweight and compliant nature of the tensegrity structure, has not been explored. To evaluate the feasibility of a thruster-based tensegrity robot, a centrally-positioned cold gas thruster with nitrogen propellant was selected, and the system was simulated using the NASA Tensegrity Robotics Toolkit (NTRT) for four hopping profiles on hilly terrains. Optimizing energy efficiency and mechanical capabilities of the tensegrity robot, hopping profiles with a long flight distance per hop, followed by the higher accuracy rolling, are recommended. Simulations also show that thrust regulation can improve energy efficiency. Regulation of thrust magnitude can be achieved using a pressure regulator, but regulation of thrust orientation calls for additional control effort. In this paper, it is demonstrated that gimbal systems as well as shape-shifting control of the tensegrity structure have the potential to regulate thrust orientation. Finally, algorithms for localization and path planning that combine hopping and rolling for energy-efficient navigation are presented.

I. INTRODUCTION

Realizing future goals in space exploration missions will require a radical change from existing architectures to allow for widespread exploration at low cost and high-reliability. This paper presents one possible concept of low-cost surface probes that can deploy small payloads with speed, robustness, and accuracy. Achieving these goals at a low cost is difficult for classical surface rovers, which are expensive to implement and require slow navigation speeds for safe operation on a planetary surface. Emerging technologies, such as hopping robots, offer quick mobility but often suffer in terms of accurate positioning or payload protection [1].

These limitations may be overcome with recent advances in spherical tensegrity robots [2], [3], [4], [5], [6], [7]. Tensegrity structures, composed of axially-loaded compression elements suspended in a network of tensional elements,

Kyunam Kim, Lee-Huang Chen, Brian Cera, Mallory Daly, Edward Zhu, Julien Despois and Alice M. Agogino are with the Department of Mechanical Engineering, University of California at Berkeley, Berkeley, CA 94720 USA {knkim, leehuanc, brianmcera, mallorycdaly, edward.zhu, despois.j, agogino}@berkeley.edu

Adrian K. Agogino is with the University of California at Santa Cruz, Santa Cruz, CA 95064 USA, and also with the NASA Ames Research Center, Moffett Field, CA 94035 USA adrian.k.agogino@nasa.gov

Vytas SunSpiral is with Stinger Ghaffarian Technologies, Inc., Greenbelt, MD 20770 USA, and is a senior researcher in the NASA Ames Intelligent Robotics Group, Moffett Field, CA 94035 USA vytas.sunspiral@nasa.gov
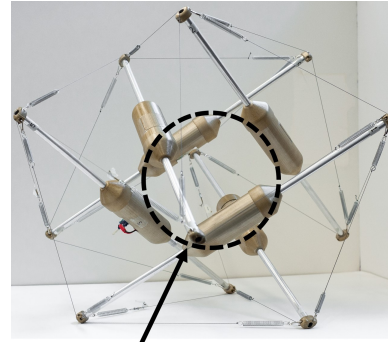
Fig. 1. A six-bar tensegrity robot, TT-3, developed at UC Berkeley. The robot has distributed controllers at the rods, clearing the center space of the structure for additional payloads, e.g., sensors or a thruster system [20].

efficiently distribute internal forces and are capable of surviving significant impact shocks upon landing [2], [8], [9], [10], [11], [12], [13], [14], [15], [16], [17]. The ball-shaped tensegrity robot, which rolls dynamically by actuating its cables, is lightweight, collapsible, and robust in difficult terrain [2], [3], [4], [5], [6], [7], [18], [19]. Additionally, its compliant structure allows it to effectively protect a delicate payload suspended at its center.

In this paper, we propose adding a simple gas thruster located near the center payload of the spherical tensegrity robot to dramatically increase the mobility of the design. The thruster will allow the robot to quickly cover long distances over difficult terrain using a series of hops while the tensegrity structure's inherent ability to distribute internal forces protects the payload. There are no lever arms in a tensegrity structure, so forces do not magnify into joints or other common points of failure. Rather, externally applied forces distribute through the structure via multiple load paths, creating a system-level robustness and tolerance to impacts and forces applied from any direction. Thus, tensegrity structures are ideally suited for operation in dynamic environments where contact forces cannot always be predicted.

To realize the thruster-based hopping concept, two technology areas have been studied: (1) mobility, allowing for safe and accurate positioning of the robot using a combination of cold gas thruster-based hopping and precision rolling; and (2) autonomy, implementing control algorithms that allow for efficient hopping and precise rolling, even in the event of unexpected obstacles or failures.

The primary goals of the tensegrity rover presented in this work are to travel by hopping and rolling over a 1 km

distance on the Moon's surface and to safely deliver a 1 kg payload. The total weight of the robot is limited to 10 kg, including the payload, in order to reduce the mission cost. These capabilities were specified by NASA for our research program and are intended to facilitate low-cost scouting missions launched as a secondary payload on a stationary lander. However, the concept is very general and can be adapted to a large number of other missions.

The Berkeley Emergent Space Tensegrities Lab at UC Berkeley, in collaboration with the Dynamic Tensegrity Robotics Lab at NASA Ames Research Center, has prototyped several state-of-the-art tensegrity robots based on a six-bar ball-shaped tensegrity structure [20], [21]. The most recent prototype, named TT-3, is shown in Fig. 1. This robot performs punctuated rolling motions by controlling cable lengths with onboard actuators to repeatedly deform, or shape-shift, its body. TT-3 has distributed controllers located in capsules at the centers of the rods, thus clearing the center space of the structure for additional payloads.

This cable-driven rolling design enables precise positioning of the robot. By adding a gas thruster, we can add the capability to quickly traverse long distances or navigate large obstacles through a series of hops. In addition, since the tensegrity is a lightweight structure (TT-3 has a mass of only 2 kg), the tensegrity robot requires only a small amount of propellant for thrust when hopping. As a result, the thruster system can be of low volume and mass, and simple cold gas propellants with low specific impulse are sufficient to provide thrust for the robot to deliver a 1 kg payload over a 1 km distance on the Moon.

II. THRUSTER EVALUATION

A number of options are available for propulsion systems, such as solid rockets, cold gas thrusters, monopropellant, and bipropellant propulsions. In this work, cold gas thrusters are chosen for the following reasons: (a) they are safe to operate in a university research setting, (b) they are of low system complexity, (c) they are inexpensive and readily available, and (d) they provide sufficient low-thrust propulsion for the hopping of lightweight tensegrity robots.

Nitrogen, helium, and carbon dioxide are the most popular propellants available for cold gas thrusters. Although helium has a high specific impulse, it also has a very low density, which necessitates a large volume for storage that is unfavorable due to size constraints. Carbon dioxide can also be problematic because it is stored in mixed gas and liquid phases, the latter needing extra care in handling. Therefore, by elimination, we focus on nitrogen thrusters.

For this concept to work, the thruster must be able to propel the tensegrity probe for a distance of 1 km over a series of hops in such a way that the payload is not damaged from excessive forces during landings. Design choices must be carefully made because large aggressive hopping could damage the payload, while small hops would be too inefficient. In this paper we analyze the feasibility of a nitrogen thruster using the design parameter values summarized in Table I. In this analysis, it is assumed that

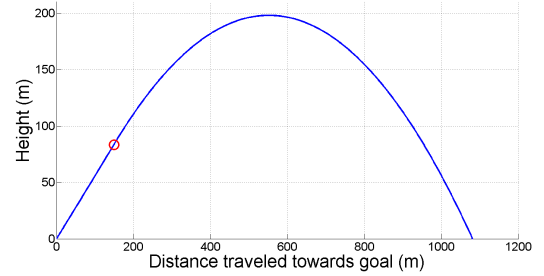| Parameters	Values	Parameters	Values
λ	0.95	a_0	204 (m/s)
P_0	2.76 (MPa)	ϵ	5
A_t	1.20e-05 (m^2)	C^*	252 (m/s)
γ	1.4	$\dot{m}$	0.132 (kg/s)
R	297 (J/kgK)	I_{sp}	46.5 (s)
T	100 (K)	F_t	50 (N)

Fig. 2. A trajectory of a thruster robot performing a single hop based on a particle mass assumption. The red circle represents the end of burning period. A constant thrust vector with its magnitude of 50 N and angle of 45 degrees is applied to simulate the trajectory.

an ideal one-dimensional nozzle is choked at its throat. The parameters include nozzle efficiency (λ), propellant mass flow rate ($\dot{m}$), specific impulse of nitrogen (I_{sp}), nozzle inlet pressure (P_0), nozzle's throat area (A_t), characteristic exhaust velocity (C^*), speed of sound in nitrogen (a_0), nozzle's expansion ratio (ϵ), specific gas constant of nitrogen (R), specific heat ratio of nitrogen (γ), temperature (T) and estimated thrust of (F_t). With the provided parameter values, a thrust of 50 N is expected from the nitrogen thruster. For a more thorough analysis on nozzle flows and thrust models, we redirect the readers to [22] and [23].

If launched at a 45-degree angle with an initial mass of 10 kg, thrust of 50 N, and burn time (i.e., the time during which the propellant is consumed) of 9 s, the robot flies more than 1 km of lateral distance on the Moon, according to a simple particle mass model (Fig. 2). The total amount of propellant required for this hopping motion is 1.19 kg, but notice that this weight is for the thermodynamic conditions provided in Table I. The total weight of the propellant needed is affected by several factors and could further be reduced, for example, by increasing the tank pressure.

Including the propellant, tank, and tensegrity structure weight, it is estimated that the total weight of the robot is below the 10 kg assumption. Therefore, it is expected that the robot will be able to travel a distance farther than what is simulated. However, with a maximum hop height of 200 m as shown in Fig. 2, the payload would receive a significant impact when landing. Having multiple, shorter distance hops can help reduce the landing velocity and thus reduce the landing impact. Analyses of several different multi-hop scenarios is discussed in Sect. III.

III. SIMULATIONS OF THRUSTER-BASED MOBILITY

Simulations in this work are performed with the NASA Tensegrity Robotics Toolkit (NTRT) [24]. NTRT is an open-source simulator developed by the Intelligence Robotics Group at NASA Ames Research Center to foster research related to tensegrity robotics. NTRT provides all of the core methods to model, simulate, and control broad types of tensegrity robots. Previous research has validated NTRT simulation result with hardware experiments [5]. Simulation of ground impact response of tensegrity robots has appeared in [20] and comparison of the impact simulation with physical hardware robots is reported in [2].

A six-bar tensegrity structure is modeled in NTRT by adopting physical parameters from UC Berkeley's rapidly prototyped robot, TT-3 (Fig. 3). To simulate thruster-based mobility, a thrust vector is applied to the center of the payload which is suspended at the center of the structure. To model real-world disturbances, noise is added to the magnitude and orientation of the thrust. The noise properties of the actual system will depend on the design of the system and environment where the robot operates. However, since the noise properties of the current system are not known at this stage, a simple Gaussian model is chosen. For every 0.1 ms of time step, thrust magnitude and orientation angles are contaminated with zero mean noise with standard deviations of 0.02 N and 0.002 radians, respectively. As a result, the thruster nozzle and thrust orientation vectors will not be perfectly aligned, and error between the two accumulates over time. This is a rather pessimistic open-loop control model that results in large positional errors. However, our results show that even under these assumptions it is possible to meet the design goals.

It should be noted that in a real system, the total mass of the robot will decrease as the robot performs hopping because of the propellant used. However, we do not consider this mass reduction in our simulations, that is, we simulate the worst case scenarios in terms of traveling distance. Moreover, our simulations showed that the effect of reducing weight on the distance traveled towards the goal is dominated by the effect of noises of thrust orientation angles. In the presence of noise, an initial error in thrust direction could cause off-track lateral motion of the robot, causing an increase in the positional error between the landing and target locations. As a result, in the absence of thrust orientation control, a distance towards the target after a hop may still be large even if the hop distance was increased due to the reducing weight. For this reason, we focus on the regulation of orientation angles, as discussed in Sect. IV.

Several options are present for possible hopping trajectories. The robot may travel the whole distance of 1 km in a single hop or it may break its path into multiple hops. The choice of the hopping trajectory depends on several factors, such as terrain conditions, presence of obstacles, and energy expenditure. In this work, four representative hopping profiles for hilly terrain conditions are considered. For each hopping profile, the nominal flight distance per hop
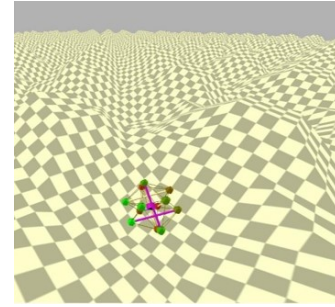

Fig. 3. A thruster tensegrity robot modeled in NTRT hilly terrain. Videos of the robot in motion are available at http://best.berkeley.edu/best-research/best-berkeley-emergent-space-tensegrities-robotics/.

is (1) 1000 m, (2) 330 m, (3) 100 m, and (4) 10 m. The required thrusts and burn times for each nominal hopping distance are first obtained with a particle mass model and then applied to the robot model in the NTRT environment. Specifically, burn times are set to 9.3 s, 5.3 s, 2.94 s, and 0.93 s for nominal hopping distances of 1000 m, 330 m, 100 m, and 10 m, respectively, with a thrust of 50 N. Examples of robot flight trajectories for different hopping profiles are presented in Fig. 4. In Fig. 4(b), a red dashed line indicates the maximum height that the robot can reach without damaging itself and its payload.

Figure 4 shows that the final location of the robot, after hopping is completed, is closer to the target as the burn time per hop (or equivalently, a nominal flight distance per hop) gets smaller because hopping resolution increases and the robot has more opportunities to correct its flying direction in between the hops. The average distances between final positions of the robot and the target over five simulations are summarized in Fig. 5 and Table II. The averages of simulated hopping distances per hop for different nominal hopping distances are presented in Fig. 6 and Table II. The robot's initial and target locations were fixed during the simulations.

During the operation of a cold gas thruster, the amount of propellant used is closely related to the total burn time. These are summarized in Table III for different hopping profiles. While a hopping profile with a greater burn time per hop tends to be more energy efficient, it is less accurate in hitting the target location (Fig. 5). This suggests that a hopping profile that is a mix of both long and short hops will not only be more energy efficient than a single long hop strategy, but also is better able to position the robot to the target location before precision rolling begins. Although the most energy-efficient, a single long hop hopping profile, such as the case shown in Fig. 4(a), is undesirable because the robot reaches a maximum height of over 150 m with this profile, and the fall from such a height may damage the robot upon landing. In [2], [25], it was shown that a tensegrity structure can survive from a 10 m drop under the Earth's gravity, in which case the terminal velocity of the robot just before hitting the ground is 14 m/s. Moreover, the structure was able to protect its center payload from the landing impact. Notice that most of the impulse the robot experiences during an impact is caused by the change in the vertical component of velocity. Under the Moon's gravity, if a body is dropped at the height of 60 m,
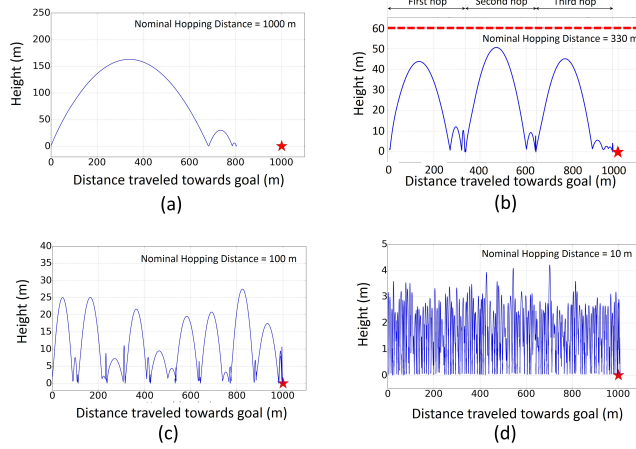
Fig. 4. Example flight trajectories of a thruster tensegrity robot on hilly terrains. The nominal hopping distances per hop are (a) 1000 m, (b) 330 m, (c) 100 m, and (d) 10 m. Red star markers represent the target location located 1000 m away from the initial position of the robot. In all figures, each hop is followed by landing bounces, resulting in additional small hops. In (a), although the average travel distance of the robot is close to 1000 m, the distance traveled towards the goal is not because of the lateral displacement it made due to angular noise of the thrust vector. In (b), a red dashed line indicates the 60 m height constraint. Once a hopping phase is over, the robot may move to the target by precision rolling.
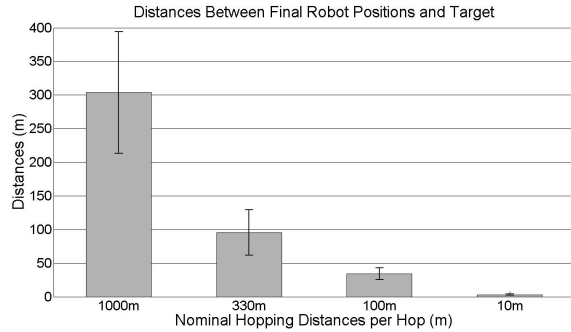

Fig. 5. Average of distances between final locations of the robot and the target after hopping phase is over. Simulations are run five times for each hopping profiles on hilly terrains assuming noise standard deviations of 0.02 N and 0.002 radians for thrust magnitude and orientation angles, respectively. The final location of the robot is closer to the target as the nominal flight distance per hop gets smaller because the hopping resolution increases and because the robot gets more chance to correct its flying direction in between the hops, but at the cost of increased energy expenditure.
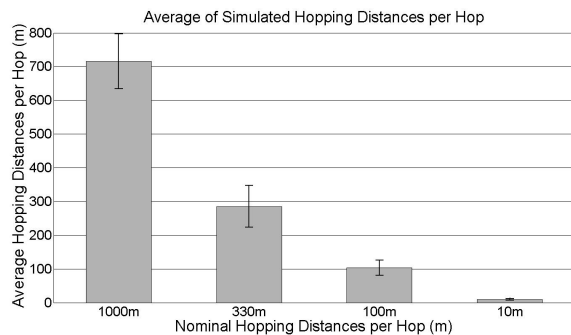

Fig. 6. Average of simulated hopping distances per hop for different nominal hopping distances. Five simulations are run for each case assuming noise standard deviations of 0.02 N and 0.002 radians for thrust magnitude and orientation angles, respectively. The average hopping distances are not equal to the nominal hopping distances due to the noise.

Nominal Hopping Distances (m)	Average of total number of hops performed to the target	Average of simulated hopping distances per hop (m)	Average distance between final robot positions and the target after hopping is done (m)
1000	1	715.3	303.8
330	3.8	285.2	95.4
100	10	103.7	34.0
10	111.4	9.6	2.9

Nominal flight distance per hop	1000 m	330 m	100 m	10 m
Total burn time to reach target	9.3 s	20.1 s	29.4 s	103.6 s
Consumed propellant mass	1.23 kg	2.65 kg	3.88 kg	13.68 kg

its final velocity just before hitting the ground is 14 m/s. Therefore, we limit the robot's flight trajectory to stay below a maximum height of 60 m for safe landing. According to the first principle particle mass model, this corresponds to a nominal burn time of 5.3 s and a nominal flight distance of 330 m per hop with a 50 N of thrust. Fig. 4(b) shows an example of such a hopping profile consisting of three hops. The variation of the peak heights is the consequence of noise in the thrust magnitudes and orientations that was added to the simulations. With this profile, the robot, on average, was able to reach a point 95.4 m away from the target on hilly terrains. From this point, the robot can roll towards the target.

Lastly, we note that the time required for the robot to arrive at the target location was not considered when comparing different hopping profiles because the traveling time is not a primary constraint in our mission. In general, a hopping profile with a shorter hopping distance per hop takes longer time to finish the hopping stage because the robot spends more time adjusting its orientation between hops.

IV. THRUSTER ORIENTATION CONTROL USING GIMBALS AND CABLE ACTUATION

Since our system can make multiple hops, it can correct for errors caused by using simple thruster control systems. In fact, in our previous simulations, feedback control was not utilized. However, when simulating this system with a reasonable degree of trajectory noise, it was observed that the trajectories of the robot were not necessarily the most efficient. An error in the initial thrust direction could cause the robot to be off-track, wasting part of its propellant in moving towards an undesirable direction. This behavior is also expected to occur in a real-world system, and the need for thrust orientation control arises for energy-efficient
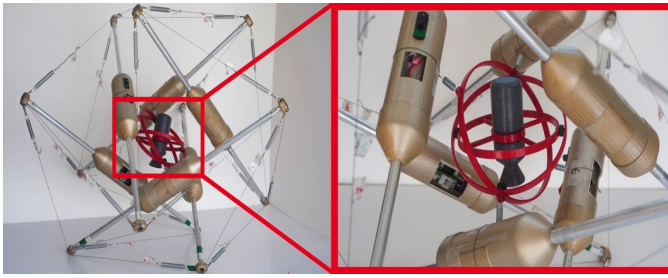
Fig. 7. A mockup of a gimbal-enclosed thruster system located at the center of the robot. Red and grey parts are mockups of a gimbal and cold gas thruster, respectively. The gimbal-enclosed thruster is connected to the robot structure with springs. The orientation control algorithm guarantees that the nozzle exit flow does not interfere with the gimbal and robot structure.
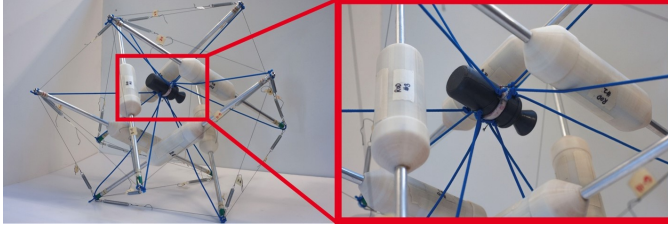

Fig. 8. A mockup of a cold gas thruster system is at the center of the robot through cable connections to outer tensegrity structure. The thruster orientation is controlled by changing the shape of the robot structure by using the shape-shifting capability of the structure.

operation of the robot. Furthermore, thrusting the robot will cause deformation in the outer tensegrity structure, which in turn can introduce additional disturbance to the thrust orientation. To address these issues, the development of suitable controls for changing thruster orientation while hopping is crucial. Three high level approaches for adjusting the thruster direction during a hopping event are being investigated:

(1) Install a two degree of freedom gimbal at the nozzle of the thruster. This will be referred to as a *gimbaled-nozzle thruster*. Gimbaled-nozzle thruster systems are well researched in rocketry and space flight for flight direction control. One of the designs that will allow for a gimbaled-nozzle thruster is the Canfield joint system [26]. It is a compact and efficient mechanism that provides a full hemisphere of motion. Since only the low-mass nozzle is controlled with the gimbal, the torque requirement is expected to be small.

(2) Another concept is to enclose the tank and thruster nozzle inside of a two degree of freedom gimbal structure. This will be referred to as a *gimbal-enclosed thruster system*. The gimbal-enclosed thruster system allows the thruster a much larger range of motion in comparison to the gimbaled-nozzle thruster system. This concept was modeled and prototyped using a 3D printer as shown in Fig. 7 to understand the large range of motion and visualize the payload size and spacing within the tensegrity robot. The gimbal-enclosed thruster system can be useful when the robot has to adjust the thruster orientation for hopping but it cannot do so by moving its whole body due to its environment, e.g. when the robot is stuck in a crater. Moreover, this concept allows not only the thruster but also the payload to utilize the gimbal system. For example, this setup will enable an imaging payload to rotate and sweep within the gimbal system.

(3) The third concept that is being explored for controlling the thruster orientation is a *cable-actuated thruster system*, which utilizes the inherent shape-shifting capability of the outer tensegrity structure. This method leverages the intrinsic high-degree of freedom present in an active tensegrity robotic probe. In the simplest form of this system, the thruster and payload would be connected to the ends of the tensegrity rods by fixed-length compliant cables as shown in Fig. 8 and orientation control would be achieved by changing the shape of the structure. In a more flexible version of this concept, additional actuation would be added to the support cables of the payload to allow for more control through shape changing. The cables that constitute the outer structure are referred to as outer cables, and the payload-suspension cables are referred to as inner cables. With this approach, the cable-actuated thruster can change its orientation by controlling the lengths, or equivalently tensions, of inner and outer cables. This approach has an advantage over the gimbal-enclosed thruster system discussed in the previous section in that there is no need to add an additional gimbal system at the center of the structure and the center space can be fully used for installation of a payload.

Since tension is distributed in a highly coupled and nonlinear manner across tensegrity members, it is difficult to predict how the tension change will affect the thruster orientation. To examine the validity of this approach, a workspace analysis (i.e., range of thruster orientation angles that can be achieved using cable-actuation) is performed. To do this, a set of target rest lengths of the structure's cables are randomly sampled and applied to a tensegrity dynamics simulation based on [27] to find one terminal structure shape and final thruster orientation. However, the sample is discarded if the final structure shape places the center of mass outside of its ground-contacting polygon. Such a shape is expected to make the robot to perform punctuated rolling [28] and as a result, the thruster will point towards a wrong direction even after the desired shape-shifting. This procedure is then repeated until enough samples are obtained that would represent a good estimation on the region of thrust angles that could be achieved with cable actuation. In the current analysis, gravitational effects are neglected and collision detection of structural members is not considered, as the main objective of the analysis is to formulate an initial conception on possible ranges of thrust angles.

In Fig. 9, three different cases are considered: (a) only inner cables are actuated, (b) only outer cables are actuated, and (c) both inner and outer cables are actuated. The initial azimuthal and elevation angles of the thrust orientation are 0 and 90 degrees, respectively. The ranges of these angles after cable actuation are summarized in Table IV.

In Table IV, the range is the widest when both inner and outer cables are actuated because the amount of shape-shifting is the greatest in this case. The range of thrust orientation angles achieved by inner cable actuation is wider than that achieved by outer cable actuation. However, inner cable actuation requires additional actuators and electronics, while outer cable actuation can be performed with the
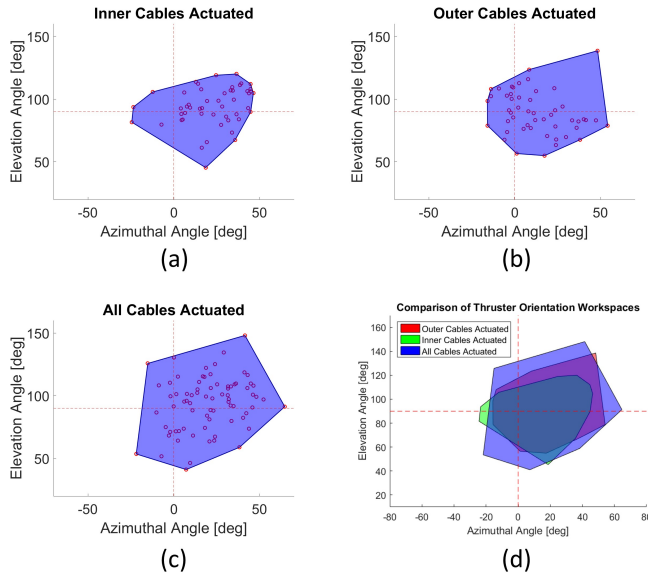
Fig. 9. Expected ranges of thrust orientation angles estimated with random sampling. Initial azimuthal and elevation angles are 0 and 90 degrees, respectively. (a) Only inner cables are actuated. (b) Only outer cables are actuated. (c) Both inner and outer cables are actuated. (d) Comparison of the three workspaces.

TABLE IV

RANGES OF THRUST ORIENTATION ANGLES FOR THREE DIFFERENT

CASES IN FIG. 9. UNITS ARE IN DEGREES.

Actuation Location	Inner cables	Outer cables	All cables
Min. azimuthal	-27	-17	-22
Max. azimuthal	46	55	63
Azimuthal difference	73	72	85
Min. elevation	44	54	42
Max. elevation	120	140	147
Elevation difference	76	86	105

existing actuators used for punctuated rolling, thereby avoiding any additional components. This difference is critical when considering the 10 kg mass restriction that competes with the benefit of having a wider range of orientation angles with inner cable actuation. For this reason, control of thrust orientation solely through outer cable actuation seems the most promising for this system. A downside to this approach is that the orientation error may be larger than the other two concepts using gimbals. In addition, the achievable workspace could be smaller and the control and actuation complexity could be higher. When a desired thrust orientation is outside of the achievable workspace, the robot may perform punctuated rolling in order to change its pose until the desired thrust orientation falls under the region of the workspace. The robot can then change its cable tension to control the thrust orientation.

While the analysis presented above provides estimated ranges of the thruster orientation achievable with cable actuation, it does not tell us how much tension should be provided to the cables given a desired thruster orientation. One possible way to approach this problem is to make use of the random samples generated for the workspace analysis. That is, we find the sample that is the closest to the desired

orientation in both azimuthal and elevation angles. Then we apply the set of target rest lengths that generated the sample. The final thruster orientation achieved with this method will not precisely match the desired target orientation, but the error between the two orientations will become negligible if the total number of samples is large and if the samples are distributed evenly over the workspace.

For all of the orientation control mechanisms introduced above, the nozzle exit flow may interfere with the robot structure during the burning period. It is important to avoid this interference because otherwise it may cause damage to the robot structure and result in mission failure. One possible solution to this problem is to predict the gas flow path based on the controlled thrust orientation and deform the robot's outer structure such that the structural components are placed farther away from the predicted gas path. This approach requires the knowledge of the robot's body shape and leads to a state estimation problem of a tensegrity robot, which is an actively studied problem as in [29].

V. LOCALIZATION AND PATH PLANNING

The primary goal of the tensegrity probe in this work is to reach a target location that is 1 km away from its initial location on the Moon. Up until this point, it has been shown that a ball-shaped tensegrity robot can utilize both rolling and hopping for its movement. We now discuss how to combine these separate motions for energy-efficient navigation.

For a realistic analysis, we consider the map of actual lunar surface in this section instead of a structured hilly terrain that we considered in earlier sections. The map of the mission surface is assumed to be readily available and divided into a grid to represent the environment, with each grid cell representing a square patch with local height information. This representation allows importing height maps directly into the simulation to test the algorithm on real data. Before the robot can plan its path and actions to reach the goal, it first localizes itself on the given map. To this end, the robot relies on a dynamically updated belief space that represents the probability of the robot being at a specific position. Initially, the probability is uniformly distributed across all possible positions in the map. Assuming that the robot can sense the height of the four neighbor cells east, west, north, south the robot updates its belief map by examining which cells on the map have their neighbors with approximately the same heights. After having its beliefs updated, the robot rolls one step in a direction and repeats the process until it is confident enough of its position (Fig. 10). In addition to finding the robot's initial position, this method can also be used to precisely locate itself on the map after hopping which may deteriorate the robot's estimation of its position due to thruster noises and secondary rolling after landing.

Once the robot's position is known, we use the A-star search algorithm [30] with the Euclidean distance to the goal as a heuristic to find the most energy efficient path (Fig. 11). The cost function consists of several components, each of which defines the cost of different actions (e.g., rolling and hopping) based on the travel distance with the

actions. For hopping motion, an additional constraint on the height difference between the robot's initial and final positions is considered in order to prevent damaging of the robot from hard impact.

At each iteration, the robot can move to any of the eight adjacent grid cells by punctuated rolling. This movement is practical only if the difference of height between the two cells is not too important. Otherwise, the robot might not be able to climb, e.g., a steep hill and the cost of taking this action will be significant. On the other hand, because going downhill requires less energy than going uphill or moving on a flat terrain, the robot will exploit this in planning its path. Thruster-based hopping allows a wider range of movement directions and distances. While more expensive than punctuated rolling, hopping is unavoidable in some cases, e.g., when the robot needs to escape from a crater with steep slopes. Although the hopping motion increases the average number of nodes reachable from each location, the A-star algorithm tries to limit the number of nodes expanded in order to reduce the computation effort.

In practice, the robot may fail when trying to execute a movement. To incorporate such failures, we define the possible outcomes of the movement along with their probabilities to happen. Since the A-star algorithm is not designed to handle random errors, the robot takes the following sequence to prevent itself from drifting too much: 1) The robot computes the best path to reach the goal from its current position. 2) The robot takes the first K actions according to its plan. Some actions may fail. 3) The robot localizes itself again after K actions. 4) The robot re-computes the best path for the remaining distance. 5) The robot lowers K to improve its accuracy near the goal. 6) The above are repeated until the robot arrives at the goal.

VI. Conclusions and Future Research

We have presented a ball-shaped tensegrity robot that combines hopping and rolling to travel from one location to the other in an energy-efficient manner, focusing on applications in lunar exploration missions. Lightweight tensegrity robots are especially suitable for hopping motions in comparison to other conventional rigid body robots because they can withstand significant impacts at the end of each hop without damaging itself or its payload. We have chosen nitrogen cold gas thrusters as our propulsion system because they are inexpensive, safe to operate, and they yield low system complexity, yet still provide sufficient thrust for the hopping of lightweight tensegrity robots. Based on simulations, it has been shown that hopping with a thruster is a feasible method for long distance travel in short durations of time.

Moreover, our simulations revealed that, in order to maximize the energy efficiency of the thrusters with limited amount of propellant, it is necessary to have a control mechanism that regulates the orientation of the thruster. We proposed to use gimbals for this purpose in two different ways: gimbaled-nozzle and gimbal-enclosed thrusters. Gimbals are well-known for many years in space industry and are proven to be effective in controlling orientation of a body.
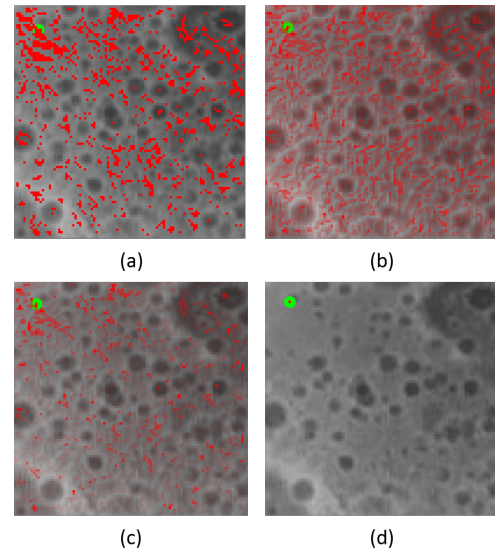

Fig. 10. Evolution of the robot's belief map while localizing itself with the known lunar surface map. Red areas represent the robot's estimated positions and green dot is the robot's true location. (a) Belief map after first measurement of neighbor grid heights. (b) Belief map after performing one step of punctuated rolling. (c) Belief map after measuring new neighbor grid heights. (d) Belief map at the end of localization process. Notice that the red areas shrank into the location of the green dot. That is, the robot successfully localized itself on the lunar map.
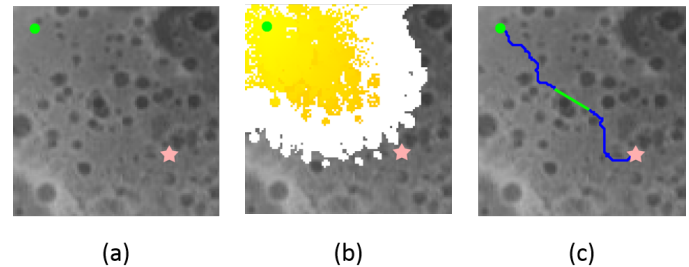

Fig. 11. (a) A lunar terrain map with height information with initial and goal locations marked with green dot and pink star, respectively. (b) A-star algorithm is used to search for the best path to the goal position. Yellow nodes are those already expanded while white nodes are those to be expanded. The shade of the yellow nodes is proportional to the cost to reach the grid cell. (c) The planned path and actions. Blue and green represent paths covered with punctuated rolling and hopping, respectively.

However, when applied to tensegrity robots, they require additional space at the center of the structure and additional actuation systems.

On the other hand, we have shown that cable-actuation of tensegrity robots is also promising in controlling the orientation of the thruster. This approach does not require any additional components as they use the actuation system already existing on the robot used for rolling locomotion. As a result, the approach can help in reducing system complexity and weight, but at the cost of complicated control algorithms. In the future, we plan to perform a trade study over the three thrust orientation control mechanisms and identify and further investigate the most promising option.

The complete mission profile of the thruster tensegrity is a combination of hopping and rolling motions. We have implemented A-star algorithm to find a feasible path of the robot from its initial location to the goal location, which also

minimizes energy consumption by appropriately combining hopping and rolling motions under the given terrain conditions. Furthermore, the robot localizes itself on a given lunar map by measuring heights of its surroundings and comparing that to its knowledge of terrain. Considering that the robot's motion always accompanies uncertainties, this localization method will greatly help the robot to re-calculate right path to the target after it makes several moves by precisely correcting its current location.

To achieve all these proposed methods of controlling the thruster system and navigating through uneven terrains, a robust sensing system is needed. The current TT-3 robot lacks feedback systems to accurately inform the controller of the state of the robot. In order to successfully execute space missions where human support is limited, the robot requires a high-level feedback controller as well as sensors to gather information about surroundings. For example, different types of sensors such as inertial measurement units and imaging devices are currently being evaluated for successfully controlling the robot during thruster hopping and rolling.

ACKNOWLEDGMENT

REFERENCES

[1] Boston Dynamics. SandFlea-leaps small buildings in a single bound. [Online]. Available: http://www.bostondynamics.com/robot_sandflea.html

[2] A. K. Agogino, V. SunSpiral, and D. Atkinson, "Super Ball Bot – structures for planetary landing and exploration," *NASA Innovative Advanced Concepts (NIAC) Program, Phase 1, Final Report*, Jul. 2013.

[3] J. Bruce, K. Caluwaerts, A. Iscen, A. P. Sabelhaus, and V. SunSpiral, "Design and evolution of a modular tensegrity robot platform," in *Robotics and Automation (ICRA), 2014 IEEE International Conference on*, 2014.

[4] J. Bruce, A. Sabelhaus, Y. Chen, D. Lu, K. Morse, S. Milam, K. Caluwaerts, A. M. Agogino, and V. SunSpiral, "SUPERball: Exploring tensegrities for planetary probes," in *Proceedings of 12th International Symposium on Artificial Intelligence, Robotics and Automation in Space (i-SAIRAS 2014)*, Montreal, Canada, Jun. 2014.

[5] K. Caluwaerts, J. Despraz, A. Işçen, A. P. Sabelhaus, J. Bruce, B. Schrauwen, and V. SunSpiral, "Design and control of compliant tensegrity robots through simulation and hardware validation," *Journal of The Royal Society Interface*, vol. 11, no. 98, 2014. [Online]. Available: http://rsif.royalsocietypublishing.org/content/11/98/20140520.abstract

[6] A. Iscen, A. K. Agogino, V. SunSpiral, and K. Tumer, "Robust distributed control of rolling tensegrity robot," in *The Autonomous Robots and Multirobot Systems (ARMS) Workshop at AAMAS*, vol. 2013, 2013.

[7] A. P. Sabelhaus, J. Bruce, K. Caluwaerts, Y. Chen, D. Lu, Y. Liu, A. K. Agogino, V. SunSpiral, and A. M. Agogino, "Hardware design and testing of SUPERball, a modular tensegrity robot," in *Proceedings of The 6th World Conference of the International Association for Structural Control and Monitoring (6WCSCM)*, Barcelona, Spain, Jul. 2014.

[8] T. Flemons. Intension designs biotensegrity models. [Online]. Available: http://www.intensiondesigns.com/models.html/

[9] B. Fuller, "Tensegrity," *Portfolio Artnews Annual*, vol. 4, pp. 112–127, 1961.

[10] S. M. Levin, "The tensegrity-truss as a model for spine mechanics: biotensegrity," *Journal of mechanics in medicine and biology*, vol. 2, no. 03n04, pp. 375–388, 2002.

[11] A. Pugh, *An introduction to tensegrity*. Univ of California Press, 1976.

[12] R. E. Skelton, R. Adhikari, J.-P. Pinaud, W. Chan, and J. Helton, "An introduction to the mechanics of tensegrity structures," in *Decision and Control, 2001. Proceedings of the 40th IEEE Conference on*, vol. 5. IEEE, 2001, pp. 4254–4259.

[13] R. E. Skelton, "Dynamics and control of tensegrity systems," in *IUTAM Symposium on Vibration Control of Nonlinear Mechanisms and Structures*. Springer, 2005, pp. 309–318.

[14] K. D. Snelson, "Continuous tension, discontinuous compression structures," Feb. 16 1965, US Patent 3,169,611.

[15] A. Tibert and S. Pellegrino, "Review of form-finding methods for tensegrity structures," *International Journal of Space Structures*, vol. 18, no. 4, pp. 209–223, 2003.

[16] J. M. Mirats Tur and S. H. Juan, "Tensegrity frameworks: Dynamic analysis review and open problems," *Mechanism and Machine Theory*, vol. 44, no. 1, pp. 1–18, 2009.

[17] V. SunSpiral, A. K. Agogino, and D. Atkinson, "Super Ball Bot – structures for planetary landing and exploration," *NASA Innovative Advanced Concepts (NIAC) Program, Phase 2, Final Report*, Sep. 2015.

[18] M. Shibata, F. Saijyo, and S. Hirai, "Crawling by body deformation of tensegrity structure robots," in *Robotics and Automation, 2009. ICRA'09. IEEE International Conference on*. IEEE, 2009, pp. 4375–4380.

[19] Y. Koizumi, M. Shibata, and S. Hirai, "Rolling tensegrity driven by pneumatic soft actuators," in *Robotics and Automation (ICRA), 2012 IEEE International Conference on*. IEEE, 2012, pp. 1988–1993.

[20] L.-H. Chen, K. Kim, E. Tang, K. Li, R. House, E. Jung, A. M. Agogino, A. K. Agogino, and V. SunSpiral, "Soft spherical tensegrity robot design using rod-centered actuation and control," in *ASME 2016 International Design Engineering Technical Conferences & Computers and Information in Engineering Conference (IDETC/CIE 2016)*. ASME, 2016.

[21] K. Kim, A. K. Agogino, D. Moon, L. Taneja, A. Toghyan, B. Dehghani, V. SunSpiral, and A. M. Agogino, "Rapid prototyping design and control of tensegrity soft robot for locomotion," in *Proceedings of 2014 IEEE International Conference on Robotics and Biomimetics (ROBIO2014)*, Bali, Indonesia, Dec. 2014, *Finalist Best Student Paper*.

[22] J. D. Anderson Jr, *Fundamentals of aerodynamics*. Tata McGraw-Hill Education, 2010.

[23] J. J. Sellers, W. J. Astore, R. B. Giffen, and W. J. Larson, *Understanding space: An introduction to astronautics*. Primis, 2000.

[24] NASA tensegrity robotics toolkit. [Online]. Available: http://irg.arc.nasa.gov/tensegrity/NTRT/

[25] A. Deng, G. Paulson, J. Saltz, and A. Savinov, "Analysis of impact absorption of a tensegrity structure," *Internal Report, UC Berkeley*, May 2013.

[26] J. Beno, "Canfield joint - vibration isolation system for high precision pointing," *Center for Electromechanicas, Univ. Texas, Proposal 11-2 T3.01-9950*, 2011.

[27] R. E. Skelton and M. C. de Oliveira, *Tensegrity systems*. Springer, 2009.

[28] K. Kim, A. K. Agogino, A. Toghyan, D. Moon, L. Taneja, and A. M. Agogino, "Robust learning of tensegrity robot control for locomotion through form-finding," in *Proceedings of 2015 IEEE/RSJ International Conference on Intelligent Robots and Systems (IROS2015)*. IEEE, 2015, pp. 5824–5831.

[29] K. Caluwaerts, J. M. Friesen, J. Bruce, and V. SunSpiral, "State estimation for tensegrity robots," in *Proceedings of 2016 IEEE International Conference on Robotics and Automation (ICRA2016)*, May 2016.

[30] S. J. Russell, P. Norvig, J. F. Canny, J. M. Malik, and D. D. Edwards, *Artificial intelligence: a modern approach*. Prentice hall Upper Saddle River, 2003, vol. 2.